JOURNAL OF PROPULSION AND POWER
Vol. 24, No. 2, March–April 2008

Use of Condensed-Phase Reaction Models in Combustion Simulation of Energetic Materials

Jun Wang* and Charles A. Wight†
University of Utah, Salt Lake City, Utah 84112-0850

DOI: 10.2514/1.27312

The contribution of condensed-phase reaction kinetics to the overall combustion behavior of cyclotetramethylenetetranitramine is investigated in the context of a successful two-step chemical reaction scheme introduced by Ward, Son, and Brewster ("Role of Gas- and Condensed-Phase Kinetics in Burning Rate Control of Energetic Solids," *Combustion Theory and Modelling*, Vol. 2, No. 3, 1998, pp. 293–312; also "Steady Deflagration of HMX with Simple Kinetics: A Gas Phase Chain Reaction Model," *Combustion and Flame*, Vol. 114, Nos. 3–4, 1998, pp. 556–568). We derive extensions of the activation energy asymptotics of the condensed-phase reaction from *n*th-order ($0 \le n \le 1$) kinetics to include 10 additional analytic reaction models. The results show that it is not possible to determine uniquely the condensed-phase reaction model by validating against steady-state burn rates and surface temperatures because the parameters of all models are sufficiently flexible to fit the experiments. However, the frequency-dependent transient response functions of mass burning rate to fluctuations in pressure and external radiation are somewhat more sensitive to the choice of kinetic model. The sensitivity of using different kinetic models to fit experimental T-burner data is more pronounced under conditions in which the surface temperature is low and no external radiation is applied. The power law model, which has the highest contribution to condensed-phase heat release, provides the best fit to transient combustion response functions.

Nomenclature

A_c	=	Arrhenius preexponential factor
B_g	=	gas-phase frequency factor
C_p	=	heat capacity
D_g	=	gas-phase Damköhler number
E	=	activation energy
f	=	frequency of oscillating pressure/radiance
f_r	=	fraction of external radiation absorbed below surface reaction zone
$f(Y)$	=	condensed-phase reaction model
K_a	=	laser absorption coefficient of condensed phase
k	=	nondimensional temperature sensitivity
m	=	mass burning rate or mass flux
m_r	=	reference mass flux, 1 $\mathrm{kg/m^2 \cdot s}$
n	=	order of reaction
P	=	pressure
Q	=	heat release
q	=	heat flux
R	=	ideal gas constant
R_p	=	pressure-driven frequency response function
R_q	=	radiation-driven frequency response function
r	=	$(\partial \overline{T}_s/\partial T_0)_p$
r_b	=	linear burn rate
T	=	temperature
W	=	molecular weight
x	=	distance
x_g	=	gas flame characteristic thickness
Y	=	mass fraction
Y_{cc}	=	critical mass fraction at burning surface
α	=	extent of conversion
δ	=	$\nu r - \mu k$, Jacobian parameter
$\partial_x y$	=	$\partial y/\partial x$
κ	=	thermal conductivity
λ	=	homogeneous solution to energy equation with oscillating perturbation
ν	=	pressure exponent or pressure sensitivity
ρ	=	solid density
σ_p	=	temperature sensitivity
Ω	=	nondimensional frequency
Ω_c	=	rate of condensed-phase reaction
ω	=	$2\pi f$, circular frequency

Subscripts

c	=	condensed phase
f	=	flame
g	=	gas
l	=	liquid
r	=	radiation
s	=	surface
α	=	extent of conversion
0	=	initial

Superscript

$\sim$	=	nondimensional quantity

Introduction

SCIENCE-BASED computer simulations of energetic material combustion are important tools for improving the safety and performance of systems like solid rocket motors and explosive devices. Simulation of small domains, often with reduced dimensionality, has allowed the development of detailed models that account for the underlying combustion chemistry and physics [1,2]. Progress in this field has been especially good for understanding the gas-phase flame chemistry. Simulations of large system-level domains with complex geometries, on the other hand, require much faster computation at lower spatial resolution using simplified combustion modeling algorithms. The weakest link in all combustion simulation is the treatment of condensed-phase reactions. This is due to the difficulty of accounting for complex physicochemical processes in the condensed phase, which occur very rapidly in a thin layer at the burning surface. As a result, all

Received 15 August 2006; revision received 21 August 2007; accepted for publication 2 September 2007.

*Research Fellow, Chemistry Department; junwang@chem.utah.edu.
†Professor, Chemistry Department; wight@chem.utah.edu.

existing combustion simulations use simple zero-order or first-order reactions to treat condensed-phase reactions.

In contrast, there is plenty of evidence that condensed-phase reactions of energetic materials are often quite complex. Most propellants are composite mixtures of oxidizer, fuel, binder, cross-linker, and plasticizers, which may react in different temperature ranges and give the burning surface a dynamic structure [3–5]. Even for monopropellants, the reaction zone at the burning surface is complicated physically and chemically by the complex nature of the condensed-phase reactions. Scanning electron micrographs show that cyclotetramethylenetetranitramine (HMX) crystals become highly porous during decomposition below the melting point [6,7]. This porosity leads to an increase in the surface area of the crystal available for reaction and accounts for the apparently autocatalytic nature of the reaction. Vyazovkin and Wight investigated the thermal decomposition of HMX using isoconversional analysis, and confirmed the complex nature of the kinetics [8]. They tried a large number of reaction models to fit the thermogravimetric data and concluded that the best fits are obtained with sigmoidal-type models rather than simple zero-order or first-order reaction models.

In 1998, Ward et al. (WSB) introduced a one-dimensional analytic steady-state combustion model based on a simplified two-step reaction scheme, i.e., a simple zero-order condensed-phase reaction followed by a second-order chain reaction in the gas phase [9,10]. The derivation of the analytical solution of the steady burn rate is achieved with activation energy asymptotics (AEA) proposed by Lengelle [11] for the condensed-phase reaction, and by setting the effective activation of the gas-phase flame reaction to zero. Perhaps surprisingly, the WSB model provides good predictions for most key combustion properties such as temperature profile, temperature sensitivity, and pressure exponent, which other models (even models with detailed chemistry) fail to reproduce.

Because it offers the dual advantages of computational simplicity and excellent predictive capability, the WSB model was adapted for use in Uintah, a massively parallel high-performance simulation code developed by the University of Utah Center for Simulation of Accidental Fires and Explosions (C-SAFE).[‡] Uintah is a problem-solving environment designed for large-scale simulations of energetic systems evolving with large deformations at high strain rates (e.g., explosions). Use of the WSB approach to predicting the combustion properties of energetic materials at the grid level provides the computational speed to simulate large domains with moderate accuracy. However, the original WSB formulation included only zero-order kinetics for the condensed-phase reaction step and the question remains whether this is adequate to describe the underlying behavior of the combustion.

In this work, we use Lengelle's scheme [11] to extend the WSB model to include 10 additional kinetic models for the condensed-phase reaction step. The analytical results obtained are used to fit the various models to experimental data to assess whether it is possible to distinguish one from another, and if so, which models produce the best results.

Theoretical Formulation

Lengelle [11] performed a matched asymptotic expansion scheme for endothermic pyrolysis of vinyl polymers, which was later extended by Ibiricu and Williams [12] by including the thermal interaction of external radiant flux q with the combustion zone. Both authors used the assumption of zero-order condensed-phase reaction. This scheme was adapted by Ward et al. [9,10] in their global kinetic combustion model. In the WSB model, the condensed phase has a one-step reaction turning condensed-phase HMX into gaseous intermediates, which react in a bimolecular gas phase to produce final gas-phase products.

The species and energy conservation equations in the reactive–diffusive zone of steady-state combustion with a moving reference frame can be written as

[‡]http://www.csafe.utah.edu

Table 1 Kinetic models of condensed-phase reactions

Model	$f(Y)$	Model description
Fn	Y^n	nth-order reaction
An	$nY(-\ell_n Y)^{(n-1)/n}$	n-D Avrami-Erofeev (nucleation and growth)
R2	$2Y^{1/2}$	contracting cylinder
R3	$3Y^{2/3}$	contracting sphere
C1B	$Y[1 + K_{cat}(1 - Y)]$	first-order reaction with autocatalysis
D1	$[2(1 - Y)]^{-1}$	one-dimensional diffusion
D2	$-(\ell_n Y)^{-1}$	two-dimensional diffusion
Pn	$(n + 1)(1 - Y)^{n/(n+1)}$	nth-order power law ($n = 1, 2, 3$)

$$r_b \rho_c \frac{dY}{dx} = \Omega_c \tag{1}$$

$$r_b \rho_c C_p \frac{\partial T}{\partial x} = \kappa_c \frac{\partial^2 T}{\partial x^2} + \Omega_c Q_c + (1 - f_r) q K_a \exp(K_a x) \tag{2}$$

$$\Omega_c = \rho_c A_c \exp(-E_c/RT) f(Y) \tag{3}$$

where Ω_c is the rate of reaction. The condensed-phase reaction model $f(Y)$ determines the dependence of the reaction rate on the mass fraction of solid Y at any distance x from the burning surface. A variety of condensed-phase reaction models have been proposed [13–15], several of which are summarized in Table 1. The fraction of external radiative heat flux q absorbed below surface reaction zone is given by

$$f_r = \exp\left(-\frac{\zeta \tilde{T}_s}{\tilde{m}\tilde{E}_c}\right) \tag{4}$$

where $\zeta = 2K_a\kappa_c/m_r C_p$. This functional form was suggested by Ibiricu and Williams based on Beer's law [12], but instead of using a constant value in the original WSB model in the derivation of temperature sensitivity, pressure exponent, and radiant flux sensitivity [16,17], f_r is treated here as a function of the mass burning rate and surface temperature.

The activation energy of HMX condensed-phase reaction is high enough ($E_c/RT \gg 1$) to perform the asymptotic expansion. Equations (1) and (2) can be solved for the burning rate m whose general formula is given as

$$m^2 = \frac{A_c R T_s^2 \kappa_c \rho_c \exp(-E_c/RT_s)}{E_c\{C_1 Q_c + C_2 C_p[T_s - T_0 - (f_r q/C_p m)]\}} \tag{5}$$

where C_1 and C_2 are the coefficients of Q_c and $C_p(T_s - T_0 - f_r q/C_p m)$, respectively. The latter is the nondimensional heat required in the surface reaction zone to raise the temperature from $(T_0 + f_r q/C_p m)$ to T_s.

It can be seen from Eq. (5) that the scale of C_1 and C_2 can always be compensated by the value of A_c, which is usually used as a fitting parameter. If A_c were allowed to be optimized for each kinetic model, the degree of freedom reduces to two, i.e. A_c and the ratio C_1/C_2.

The gas-phase scheme and solution follow exactly the same as the original WSB model [9,10]. The nondimensional form of the solution is

$$\tilde{T}_s = \tilde{T}_0 + \tilde{Q}_c + \frac{\tilde{Q}_g}{x_g \tilde{m} + 1} + J \tag{6}$$

$$x_g = \frac{2}{\sqrt{\tilde{m}^2 + 4D_g} - \tilde{m}} \tag{7}$$

where D_g is the gas-phase Damköhler number

$$D_g \equiv \frac{k_g B_g P^2 MW^2}{m_r^2 R^2 C_p}$$

in which B_g is the frequency factor for the gas-phase chain reaction. The scalings are

$$\tilde{m} \equiv m/m_r, \quad \tilde{T}_s \equiv \frac{T_s}{T_f - T_0}, \quad \tilde{T}_0 \equiv \frac{T_0}{T_f - T_0}$$

$$\tilde{Q}_c \equiv \frac{Q_c}{C_p(T_f - T_0)}, \quad \tilde{Q}_g \equiv \frac{Q_g}{C_p(T_f - T_0)}$$

$$J \equiv \frac{\tilde{q}}{m} = \frac{q}{mC_p(T_f - T_0)}$$

Now we define a new parameter $C_Q \equiv C_1/C_2 + 1$. By substituting Eqs. (6) and (7) into Eq. (5), the mass burning rate, in nondimensional form, can be rewritten as

$$\tilde{m}^2 = \frac{\tilde{A}_c \tilde{T}_s^2 \exp(-\tilde{E}_c/\tilde{T}_s)}{\tilde{E}_c[C_Q \tilde{Q}_c + \tilde{Q}_g/(x_g \tilde{m} + 1) + (1 - f_r)J]} \tag{8}$$

with the following scalings: $\tilde{A}_c \equiv \kappa_c \rho_c A_c / C_p m_r$, $\tilde{E}_c \equiv E_c/R(T_f - T_0)$.

Equations (6–8) can be fit to experimental data by allowing A_c and B_g to be free parameters for each reaction model used. The advantage of expressing the mass burning rate in terms of the product $C_Q Q_c$ is that this term gives the contribution of the condensed-phase heat release to the temperature rise in the reaction zone.

In most condensed-phase reaction models, $f(Y)$ approaches 0 as $Y \to 0$, causing the rate of reaction to become infinitesimally small but never exactly zero. The power law models (P1, P2, and P3 in Table 1) and the zero-order model (F0) are important exceptions. If we divide a one-dimensional domain into grid elements having finite width, then, in principle, an infinite amount of time is required to burn out all solid material in each grid element. Consequently, the computed surface does not regress. It is therefore necessary to apply a small critical value Y_{cc} as a cutoff value for Y. Grids are considered to be completely burned if the value of Y is less than Y_{cc}. We choose a value of 0.01 for Y_{cc}, and it is determined that the value of C_Q obtained from fits to experimental data is not strongly dependent on Y_{cc} when $Y_{cc} \leq 0.01$ for the condensed-phase reaction models listed in Table 1. The analytic expressions for C_1 and C_2 (and, by inference, C_Q) are presented in Table 2 for each reaction model considered in this study.

Table 3 presents the numerical values of C_Q for different kinetic models in descending order when $Y_{cc} = 0.01$. The values of C_Q are much higher for power law models (P1, P2, and P3) than those for first- and second-order kinetic models (F1 and F2). This implies that the power law models rely more on the heat generation from condensed-phase reactions, whereas the first-order and second-order reactions depend less on the condensed-phase heat release, and more on heat conduction from the gas-phase flame reaction and external radiation, if applied.

To understand the reason for this phenomenon, it is helpful to look into the differences in the reaction zone structure produced by different kinetic models. The one-dimensional profiles of mass fraction Y and temperature T are obtained by solving Eqs. (1) and (2) with the asymptotic expansion scheme. In the absence of external radiation, the profiles of Y and T for some selected models at $P = 1$ atm are illustrated in Figs. 1 and 2, respectively. The temperature profile for thermal conduction only, i.e., no condensed-phase reactions involved, is also plotted. For the purposes of this comparison, the surface temperatures were forced to be the same for all kinetic models.

Table 3 C_Q for different kinetic models ($Y_{cc} = 0.01$)

Model	C_Q
P3	0.802
P2	0.753
P1	0.670
F0	0.505
C1B	0.414
A2	0.412
R2	0.370
D1	0.340
R3	0.318
D2	0.265
F1	0.215
F2	0.047

Figure 1 shows that the thickness of the reaction zone increases as C_Q decreases, with some crossover of the Y profiles for some models. The third-order power law model (P3) has the thinnest reaction zone, and so its temperature profile resembles a pure thermal conduction curve without heat release from the condensed-phase reactions. As a result, most of the condensed-phase heat release is used to raise the reaction zone temperature; only a small portion of the heat release contributes to increasing the temperature in the preheated zone, which is below the reaction zone. At the other extreme, the second-order reaction has the most extended reaction–diffusion zone. The condensed-phase heat release is shifted to increase the temperature of the preheated zone. In other words, to maintain the same surface temperature, more heat is needed from the gas-phase flame and/or external radiation.

The thickness of the reaction zone drops dramatically for all kinetic models when pressure increases, however, the patterns and relative thickness between these models remain unchanged. The influence of condensed-phase kinetic models is thus less pronounced at high pressures and high burn rates.

To compare the various condensed-phase reaction models, the values of A_c and B_g are first calculated analytically with Eqs. (6–8) for different kinetic models from a baseline (i.e., an experimental data point), which for this instance is chosen to be $T_0 = 298$ K, $P = 20$ atm, $m = 6.8$ kg/m^{2}s, and $T_s = 733$ K when $q = 0$ [9,10]. The best-fit values of A_c and B_g are then used to calculate m and T_s for other conditions by varying P, T_0, q, etc.

From Eqs. (4) and (6–8), we can see that the governing equations are functions with implicitly coupled variables, as shown by

Table 2 The analytical expressions for C_1 and C_2 for selected kinetic models

Model	$f(Y)$	C_1	C_2
F0	1	$-(1 - Y_{cc})^2/2$	$1 - Y_{cc}$
F1	Y	$1 - Y_{cc} + \ell n\, Y_{cc}$	$-\ell n\, Y_{cc}$
F2	Y^2	$1 - 1/Y_{cc} - \ell n\, Y_{cc}$	$-1 + 1/Y_{cc}$
A2	$2Y(-\ell n\, Y)^2$	$\sqrt{\pi} erf(\sqrt{-\ell n\, Y_{cc}})/2 - \sqrt{-\ell n\, Y_{cc}}$	$\sqrt{-\ell n\, Y_{cc}}$
R2	$2\sqrt{Y}$	$(1 - Y_{cc}\sqrt{Y_{cc}})/3 - (1 - \sqrt{Y_{cc}})$	$1 - \sqrt{Y_{cc}}$
R3	$3Y^{2/3}$	$\left(1 - Y_{cc}^{4/3}\right)/4 - \left(1 - Y_{cc}^{1/3}\right)$	$1 - Y_{cc}^{1/3}$
D1	$[2(1 - Y)]^{-1}$	$\left(1 - 3Y_{cc}^2 + 2Y_{cc}^3\right)/3 - (1 - Y_{cc})^2$	$(1 - Y_{cc})^2$
D2	$-(\ell n\, Y)^{-1}$	$\left(1 - Y_{cc}^2 + 2Y_{cc}^3\, \ell n\, Y_{cc}\right)/4 - (1 - Y_{cc} + Y_{cc}\, \ell n\, Y_{cc})$	$(1 - Y_{cc} + Y_{cc}\, \ell n\, Y_{cc})$
P1	$2\sqrt{1 - Y}$	$-(1 - Y_{cc})\sqrt{1 - Y_{cc}}/3$	$\sqrt{1 - Y_{cc}}$
P2	$3(1 - Y)^{2/3}$	$-(1 - Y_{cc})^{4/3}/4$	$(1 - Y_{cc})^{1/3}$
P3	$4(1 - Y)^{3/4}$	$-(1 - Y_{cc})^{5/4}/5$	$(1 - Y_{cc})^{1/5}$
C1B	$Y[1 + K_{cat}(1 - Y)]$	$\ell n\left\{[1 + K_{cat}(1 - Y_{cc})]Y_{cc}^{K_{cat}}\right\}/[K_{cat}(K_{cat} + 1)]$	$\ell n\{[1 + K_{cat}(1 - Y_{cc})]/Y_{cc}\}/(K_{cat} + 1)$

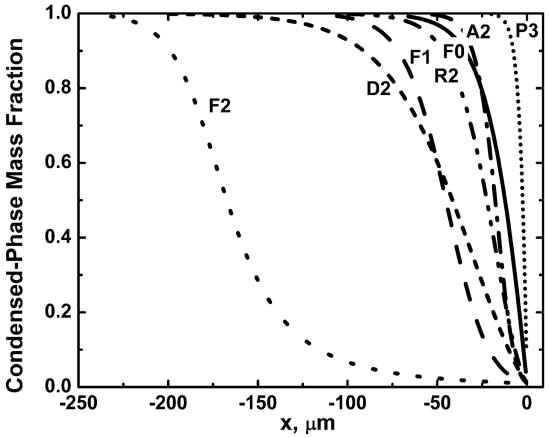

Fig. 1 Mass fraction of condensed-phase HMX at $P = 1$ atm.

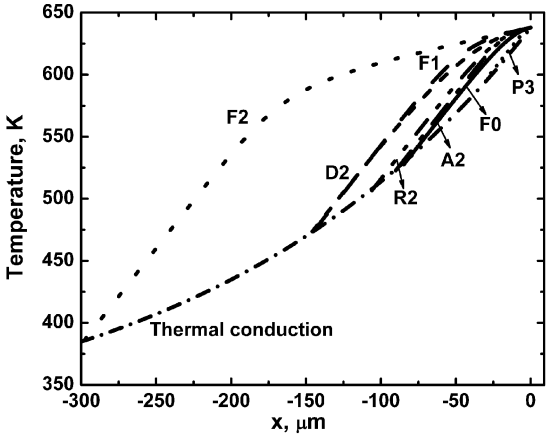

Fig. 2 Temperature profile of condensed-phase HMX at $P = 1$ atm.

$$\tilde{m} = f(\tilde{T}_0, \tilde{T}_s, \tilde{E}_c, \tilde{Q}_c, f_r, J) \qquad \tilde{T}_s = g(\tilde{T}_0, \tilde{Q}_c, \tilde{P}, \tilde{m}, J)$$
$$J = J(q, \tilde{m}) \qquad f_r = f_r(\tilde{T}_s, \tilde{E}_c) \tag{9}$$

The analytic expressions of the sensitivities of burning rate to condensed-phase and gas-phase kinetic parameters, e.g., k, ν, r, and μ, can be obtained by differentiating and solving Eq. (9). See the Appendix for the detailed derivation.

Results and Discussion

Determination of Q_c and E_c

Before we can move on to investigate the effect of using different kinetic models, two other important factors, condensed-phase heat release Q_c and activation energy E_c, need to be considered and determined for HMX combustion.

The reported heat release values for condensed-phase reaction cover a wide span. The heat release of liquid HMX thermal decomposition has been estimated to be 980 ± 40 kJ/kg (exothermic) with isothermal differential scanning calorimetry (DSC) in flowing N_2 at seven temperatures (283–289°C) [5]. This value is significantly higher than Zenin's estimation from combustion study, which is 59 kJ/kg endothermic [18]. In Zenin's report, the value of Q_c increases from −59 kJ/kg (endothermic) to 536 kJ/kg (exothermic) as pressure increases from 1 to 70 atm. Zenin's value of Q_c at high pressures may have been overestimated by underestimating the radiation flux from the high-temperature flame, in that the radiation flux decreases as pressure increases in Zenin's analysis. Tarver and Tran estimated the value of Q_c to be 264 kJ/kg, including the $\beta \rightarrow \delta$ phase transition, fragmentation, and decomposition of HMX to intermediate gas products [19].

There are at least three possible reasons for the large discrepancy of Q_c measurements from different authors. First, the condensed-phase heat release between low-temperature decomposition and high-temperature combustion may not be directly comparable due to different chemical mechanisms and correspondingly different energetics. This phenomenon is illustrated by the two-channel reaction scheme in [20], in which the two competing rate-limiting reactions have different activation energies and exothermicities. Second, DSC can not perfectly separate the condensed-phase heat release from secondary near-surface gas–solid and gas–gas reaction heat release. Finally, there are large uncertainties in the combustion measurements, especially the surface temperature, surface temperature gradient, and radiation flux from the flame.

Ward et al. [9,10] used a Q_c value of 400 kJ/kg in their WSB model. However, when external radiation is applied, the reported values of Q_c are much lower. Loner and Brewster used a value of $Q_c = 155$ kJ/kg in their WSB model with $q = 35$ W/cm^2 [21,22]. Kudva et al. [23] measured the heat release of condensed-phase reaction of laser-assisted HMX combustion at $P = 1$, 2, and 3 atm; the resulting values lie in the range of 100–200 kJ/kg. Therefore, the values of Q_c to be tested in this study are chosen to be 100–400 kJ/kg for HMX combustion without external radiant flux, and −50–300 kJ/kg for combustion with external radiant flux.

The range of reported condensed-phase activation energies are between 54 and 280 kJ/mol. Vyazovkin and Wight estimated the activation energy to be 145 kJ/mol using model-fitting analysis of isothermal decomposition of HMX [8]. Henson et al. studied the ignition time of HMX and obtained an activation energy of 149 ± 1.1 kJ/mol by fitting the ignition data to classic Arrhenius form [24]. Two values of the activation energy, 146 and 176 kJ/mol, are selected to study the effect of activation energy on the steady-state and quasi-steady HMX combustion.

The pressure sensitivity ν, or pressure exponent in the "burn law," is a critical property of HMX combustion. The experimental value of ν is 0.82 ± 0.02 in the pressure range of 1–1000 atm [5]. Figure 3 shows the effect of Q_c and E_c on the analytic solution of ν. The best fits are obtained when Q_c is 400 kJ/kg and $E_c = 146$ kJ/mol.

Temperature sensitivity σ_p is another important property because it provides information on the rate of condensed-phase reaction sensitivity to initial temperatures, defined as $\sigma_p = \partial \ln m / \partial T_0|_p = k/(T_s - T_0)$. Two measurements of temperature sensitivities are available in the literature from Zenin [18] and Atwood et al. [25]. The temperature sensitivity data from Atwood et al. are scattered at low pressures. Although it is difficult to determine the value of Q_c for each pressure due to the uncertainty of the experimental data, it can be seen from Fig. 4 that different values of Q_c fit to different pressure ranges. High Q_c (≥ 300 kJ/kg) provide the best fits for pressures lower than 20 atm, whereas Q_c is around 200 kJ/kg for pressures above 40 atm. The temperature sensitivity is almost independent of E_c in the range of 146–209 kJ/mol for $Q_c = 100$–400 kJ/kg.

Based on the model fitting of the pressure exponent and temperature sensitivity of steady-state HMX combustion, the value of Q_c decreases from 300–400 kJ/kg at $P < 20$ atm to about 200 kJ/kg at $P > 40$ atm in the absence of external radiation. This is

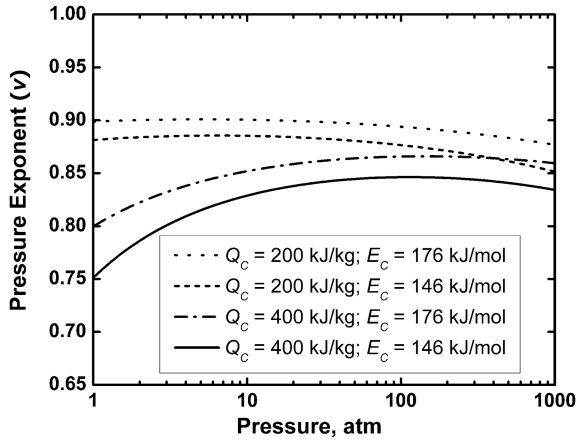

Fig. 3 Effect of Q_c and E_c on the pressure exponent ν.

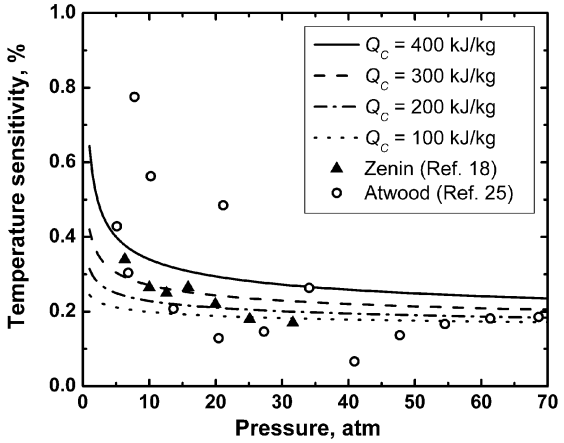

Fig. 4 Effect of Q_c and E_c on temperature sensitivity σ_p.

the same trend as found with the two-channel reaction model used by Brill et al. [20], except that their model predicts much lower, even negative, values of Q_c (endothermic process) at high pressures when the surface temperature is high.

Steady-State Combustion ($q = 0$)

Figures 5 and 6 explore the pressure and kinetic model dependence of mass burning rate and surface temperature, respectively. The values of Q_c and E_c are chosen based on the conclusion of the previous section: $Q_c = 400$ kJ/kg and $E_c =$ 146 kJ/mol. As one can see in these two figures, the fits of all kinetic

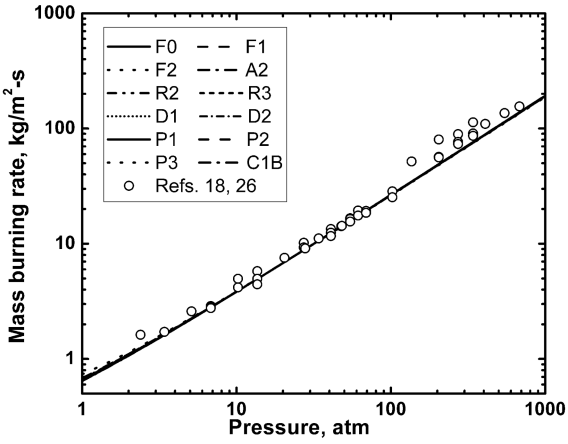

Fig. 5 Mass burning rate vs pressure for different kinetic models. All 12 models are perfectly overlapped.

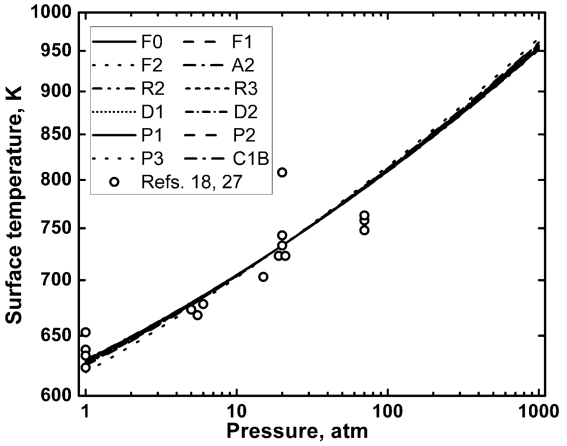

Fig. 6 Surface temperature vs pressure for different kinetic models. All 12 models are perfectly overlapped.

models to the experimental data [18,26,27] are completely indistinguishable. Therefore, if only the steady mass burning rate and surface temperature were used to validate the kinetics, no conclusion could be drawn about the nature of the condensed-phase reaction model.

Quasi-Steady Results (Zel'dovich–Novozhilov Theory, $q = 0$)

Intrinsic combustion stability can be assessed by quasi-steady, homogeneous propellants, and one-dimensionality (QSHOD) response functions. The theoretical development of the QSHOD theory has been reviewed extensively [28–30]. Two approaches have coexisted, namely the Zel'dovich-Novozhilov (ZN) method and the flame modeling (FM) theory. In the QSHOD framework, the response function of burning rate to harmonic pressure or radiation oscillations is used to describe the intrinsic combustion stability over a range of frequencies. In the linear approximation of the QSHOD theory, where a small amplitude in pressure or radiation perturbation is assumed, the analytic expressions for response functions can be derived. For instance, the response function (in ZN form) for oscillatory pressure-driven combustion is [16]

$$R_p = \frac{\nu + \delta(\lambda - 1)}{\lambda r + (k/\lambda) - (r + k) + 1} \tag{10}$$

The definitions of ν, k, and r are shown in Eqs. (A.8), (A.9), and (A.11), respectively. The intrinsic stability boundaries can be obtained by setting the denominator of the preceding response function equal to zero; the ZN form of the stability criterion is given by Eq. (11).

$$r > (k - 1)^2/(k + 1) \tag{11}$$

Son and Brewster [16] and DeLuca et al. [31] have shown that the FM and ZN approaches produce linear frequency response functions that are equivalent for both the pressure-driven and radiation-driven combustion. The intrinsic stability boundaries of the two approaches are also equivalent.

The nonlinear intrinsic combustion stability was investigated by DeLuca [30]. In that work, the stability problems related to either random transient disturbances or a permanent change of pressure/radiation was analyzed. The parabolic governing partial differential equation (PDE) for energy conservation was reformulated to an ordinary differential equation (ODE) using an integral method. A nonlinear algebraic function was then determined to study the nonlinear stability. However, the replacement of the zero-order condensed-phase reaction with other kinetic models will be far too complex for a general analytical analysis. Therefore, nonlinear intrinsic stability is not examined in this work.

Figure 7 shows the k–r plot for the results of the extended WSB model with $Q_c = 400$ kJ/kg at $P = 13.6$ atm. In the stable region, the steady-state HMX combustion can always be regained after a small perturbation of pressure. Unstable combustion of HMX has been observed at atmospheric pressure, but is stable at higher pressures. T-burner experiments have shown that HMX combustion

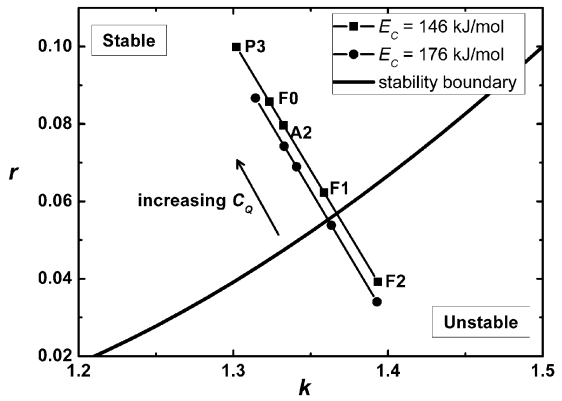

Fig. 7 Intrinsic stability of HMX combustion for selected kinetic models.

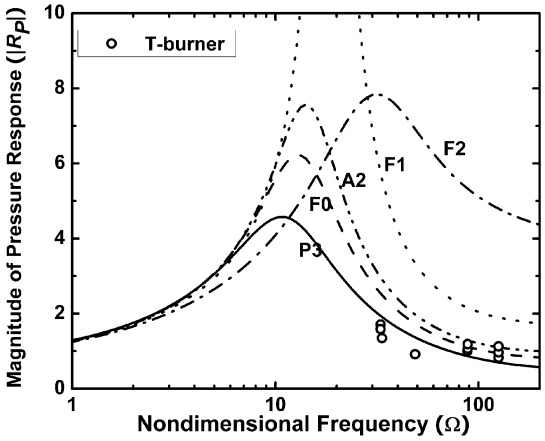

Fig. 8 Pressure response of HMX combustion at 13.6 atm ($Q_c = 400$ kJ/kg).

is in the stable zone at 13.6 and 68 atm, even for large pressure oscillations [32]. As shown in Fig. 7, the intrinsic stability of HMX combustion increases as E_c decreases and C_Q increases. Only the second-order reaction (F2) is unstable when $E_c = 146$ kJ/mol, whereas the first-order reaction is also unstable when $E_c = 176$ kJ/mol.

Figure 8 illustrates the linearized pressure response for some representative kinetic models with $Q_c = 400$ kJ/kg and $E_c =$ 146 kJ/mol, plotted against nondimensional frequency $\Omega = 2\pi f \kappa_c / C_p \rho_c r_b^2$. The effect of choosing different kinetic models is significant. The first-order reaction (F1) and second-order reaction (F2) either become very unstable or grossly overpredict the magnitude of the pressure response R_p for $\Omega = 30$–200. The magnitude of R_p decreases (closer to T-burner data) as E_c decreases from 209 to 146 kJ/mol (not shown in the figure). The third-order power law model (P3), which has the highest C_Q value, yields the best fit to T-burner data [32].

When Q_c is lowered to 300 kJ/kg with $E_c = 146$ kJ/mol, the magnitude of R_p for all kinetic models decreases, as indicated in Fig. 9. Although the difference of applying various kinetic models becomes smaller compared with the results with $Q_c = 400$ kJ/kg, it is still obvious. The P3 model again gives the best agreement to T-burner data.

The other T-burner pressure condition is 68 atm [32], which falls in the range where the estimated value of Q_c is reduced to around 200 kJ/kg from the previous discussion. The same trend is found for the effect of Q_c and E_c on the magnitude of R_p at 68 atm in the $|R_p|$ vs Ω plot (not given). However, the dependence of R_p on the condensed-phase kinetic models becomes very weak. This is because the reaction layer for all kinetic models becomes so thin that the differences of the Y profiles are much less distinguishable.

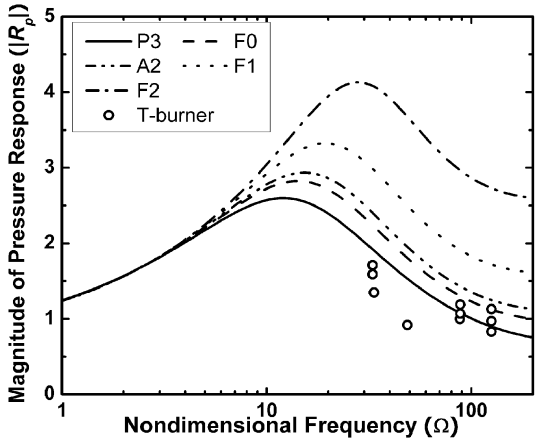

Fig. 9 Pressure response of HMX combustion at 13.6 atm ($Q_c = 300$ kJ/kg).

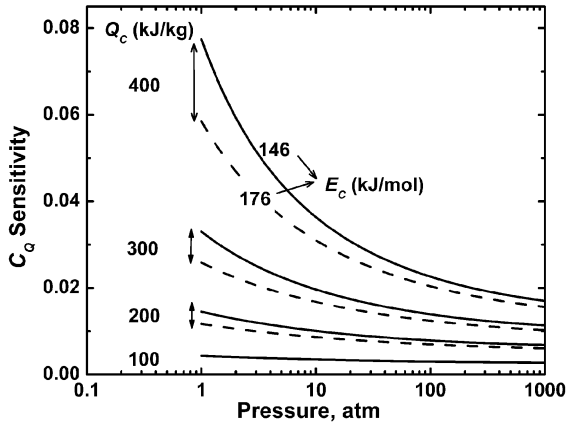

Fig. 10 Effect of Q_c and E_c on C_Q sensitivity at different pressures.

The effect of using different kinetic models in quasi-steady combustion modeling can be illustrated by the nondimensional sensitivity of burning rate to C_Q, defined as $\partial \ln \tilde{m} / \partial \ln C_Q$, because C_Q is the unique characteristic that differentiates all kinetic models in the analytic solution of the mass burning rate in this method. As one can see from Fig. 10, the burning rate of HMX is more sensitive to C_Q when the pressure is low and Q_c is high. This is due to the thicker reaction zone under these conditions, which results in more obvious differences in the Y profiles (as shown in Fig. 1) among these models. The effect of the spatial distribution of reaction rate in the one-dimensional condensed-phase combustion region becomes more observable when the reaction zone is thick and the distribution of the condensed-phase heat release matters. This is when the condensed-phase kinetic model can play a more important role in revealing the complex physiochemical surface phenomena in HMX combustion. Whereas higher values of Q_c at low pressures help to disclose the differences between different kinetic models, the activation energy E_c is also a factor in the C_Q sensitivity analysis. The HMX mass burning rate is somewhat more sensitive to the condensed-phase kinetic model when it is predicted with lower E_c.

HMX Combustion with External Radiant Flux

The mass burning rate response to oscillating external radiant flux at 1 atm was measured by Loner and Brewster [21,22]. Figure 11 illustrates the effect of Q_c and kinetics models on the response function R_q with a mean external radiant flux of 35 W/cm^2. The value of Q_c plays an important role. The predictions of both the magnitude and phase (not shown) of R_q become better as Q_c decreases from 200 to 155 kJ/kg. The best agreement can be achieved by setting $Q_c = 155$ kJ/kg and $E_c = 146$–176 kJ/mol. The effect of changing kinetic models lessens with the presence of external radiation because the laser energy reduces the relative

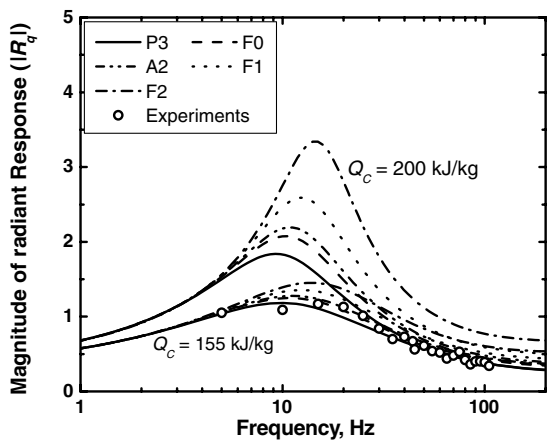

Fig. 11 Effect of Q_c and kinetic models on $|R_q|$ of HMX combustion ($q = 35$ W/cm^2; $E_c = 146$ kJ/mol).

contribution of the condensed-phase reaction to the heating of the surface zone.

Conclusions

Steady-state combustion measurements are not sufficient for drawing conclusions about the nature of the condensed-phase reaction kinetics. However, quasi-steady linear pressure response functions derived from oscillating combustion measurements can be used to determine the best values of E_c and Q_c. The best-fit value of Q_c decreases with external factors that increase the burn rate such as pressure or the presence of external laser radiation. This is the opposite trend compared with Zenin's measurements of temperature profiles [18], but is qualitatively consistent with the two-channel reaction scheme for nitramine propellants [cyclotrimethylenetrinitramine (RDX) and HMX] used by Brill et al. [20], which is based on T-jump Fourier transform infrared spectroscopy (FTIR) experiments.

The power law condensed-phase reaction model gives the best fit to quasi-steady combustion measurements. This indicates that the reaction zone is much thinner than would be predicted by simple zero- or first-order reaction models. Therefore, as more accurate and detailed combustion validation results become available, it will become necessary to incorporate more detailed condensed-phase reaction kinetics into combustion simulations. Some combustion simulation models have been developed over the past decades to include more sophisticated condensed-phase phenomena, including multistep reactions [33], phase transition [34–36], melting [37,38], porosity of the granular material [39,40], etc. However, they are either computationally expensive (not applicable to large-scale engineering simulation codes for the time being) or do not give significantly better performance than the WSB model in transient combustion simulation. Some of the kinetic models tested in this work may serve as simplified treatments of complex physicochemical processes in HMX combustion.

Appendix: Sensitivities of Burning Rate to Condensed-Phase Kinetic Parameters

It can be seen from Eqs. (4) and (6–8) that the governing equations are functions with implicitly coupled variables, as shown by

$$\tilde{m} = f(\tilde{T}_0, \tilde{T}_s, \tilde{E}_c, \tilde{Q}_c, f_r, J) \qquad \tilde{T}_s = g(\tilde{T}_0, \tilde{Q}_c, \tilde{P}, \tilde{m}, J)$$
$$J = J(q, \tilde{m}) \qquad f_r = f_r(\tilde{T}_s, \tilde{E}_c) \tag{A.1}$$

The analytic expressions of the sensitivities of burning rate to condensed-phase and gas-phase kinetic parameters can be obtained by differentiating and solving the preceding equations. With the following groupings,

$$D_1 = \tilde{A}_c \exp\left(-\frac{\tilde{E}_c}{\tilde{T}_s}\right) \qquad D_2 = C_Q \tilde{Q}_c + \frac{\tilde{Q}_g}{x_g\tilde{m}+1} + (1-f_r)J \qquad D_3 = \frac{2x_g\tilde{Q}_g}{(x_g\tilde{m}+1)(x_g\tilde{m}+2)} + \frac{J}{\tilde{m}} \tag{A.2}$$

the nondimensional sensitivity of burning rate to E_c is given as

$$\frac{\partial \ln \tilde{m}}{\partial \ln \tilde{E}_c} = \frac{\tilde{E}_c}{\tilde{m}} \frac{D_2\tilde{m}^2(\tilde{E}_c/\tilde{T}_s + 1) - \tilde{m} f_r J \zeta \tilde{T}_s/\tilde{E}_c}{D_3\tilde{m}(\tilde{m}\tilde{E}_c + f_r J\zeta) - 2D_2\tilde{m}\tilde{E}_c - f_r J(\tilde{m}\tilde{E}_c - \zeta\tilde{T}_s) - D_1D_3(2\tilde{T}_s + \tilde{E}_c)} \tag{A.3}$$

The nondimensional sensitivity of burning rate to Q_c is

$$\frac{\partial \ln \tilde{m}}{\partial \ln \tilde{Q}_c} = \frac{\tilde{Q}_c}{\tilde{m}} \frac{-D_1(2\tilde{T}_s + \tilde{E}_c) + \tilde{m}^2\tilde{E}_c C_Q + \tilde{m} f_r J\zeta}{D_3\tilde{m}(\tilde{m}\tilde{E}_c + f_r J\zeta) - 2D_2\tilde{m}\tilde{E}_c - f_r J(\tilde{m}\tilde{E}_c - \zeta\tilde{T}_s) - D_1D_3(2\tilde{T}_s + \tilde{E}_c)} \tag{A.4}$$

The nondimensional sensitivity of burning rate to C_Q is

$$\frac{\partial \ln \tilde{m}}{\partial \ln C_Q} = \frac{C_Q}{\tilde{m}} \frac{\tilde{m}^2\tilde{Q}_c}{D_3\tilde{m}(\tilde{m}\tilde{E}_c + f_r J\zeta) - 2D_2\tilde{m}\tilde{E}_c - f_r J(\tilde{m}\tilde{E}_c - \zeta\tilde{T}_s) - D_1D_3(2\tilde{T}_s + \tilde{E}_c)} \tag{A.5}$$

Other steady-state sensitivity expressions in the QSHOD framework can be derived as well. Because of the complexity of the implicitly coupled equations, algebraic manipulation of those variables (many of which are functions of other dependent variables) is required in a traditional derivation procedure. Here, the "Murphy approach" [41] is applied as a systematic procedure for deriving the QSHOD steady-state sensitivity parameters.

Equation (A.6) shows Murphy's formulation [41] for a state-space represented set of governing equations [Eq. (A.1)]. Equation (A.7) is its equivalent matrix of row-reduced form of Eq. (A.6).

$$\begin{pmatrix} \partial_{\tilde{T}_0} f & \partial_{\tilde{T}_s} f & \partial_{\tilde{m}} f & \partial_{\tilde{q}} f & \partial_{\tilde{P}} f \\ \partial_{\tilde{T}_0} g & \partial_{\tilde{T}_s} g & \partial_{\tilde{m}} g & \partial_{\tilde{q}} g & \partial_{\tilde{P}} g \\ 1 & -1 & -1 & f_r J & 0 \end{pmatrix} \begin{pmatrix} \tilde{T}_0' \\ \tilde{T}_s' \\ \tilde{m}' \\ \tilde{q}' \\ \tilde{P}' \end{pmatrix} = \begin{pmatrix} 0 \\ 0 \\ 0 \end{pmatrix} \tag{A.6}$$

$$\begin{pmatrix} k & 0 & -1 & \nu_q & \nu \\ r & -1 & 0 & \mu_q & \mu \\ 1 & -1 & -1 & f_r J & 0 \end{pmatrix} \begin{pmatrix} \tilde{T}_0' \\ \tilde{T}_s' \\ \tilde{m}' \\ \tilde{q}' \\ \tilde{P}' \end{pmatrix} = \begin{pmatrix} 0 \\ 0 \\ 0 \end{pmatrix} \tag{A.7}$$

where $'$ denotes the complex fluctuating quantity.

Owing to the equivalency of the preceding two systems and considering a set of governing equations that are expressed solely in terms of the independent variables T_0, P, and q, we can derive the general formulas for the sensitivities in terms of the partial derivatives of the governing equations. The QSHOD parameters are therefore

$$k = (\tilde{T}_s - \tilde{T}_0)\frac{\partial \ln \tilde{m}}{\partial \tilde{T}_0} = \frac{(\tilde{T}_s - \tilde{T}_0)}{\tilde{m}} \cdot \frac{\partial_{\tilde{T}_0} g \cdot \partial_{\tilde{T}_s} f - \partial_{\tilde{T}_0} f \cdot \partial_{\tilde{T}_s} g}{\partial_{\tilde{T}_s} g \cdot \partial_{\tilde{m}} f - \partial_{\tilde{T}_s} f \cdot \partial_{\tilde{m}} g} \tag{A.8}$$

$$\nu = \frac{\partial \ln \tilde{m}}{\partial \ln \tilde{P}} = \frac{\tilde{P}}{\tilde{m}} \cdot \frac{\partial_P g \cdot \partial_{\tilde{T}_s} f - \partial_P f \cdot \partial_{\tilde{T}_s} g}{\partial_{\tilde{T}_s} g \cdot \partial_{\tilde{m}} f - \partial_{\tilde{T}_s} f \cdot \partial_{\tilde{m}} g} \tag{A.9}$$

$$\nu_q = \frac{\partial \ln \tilde{m}}{\partial \ln \tilde{q}} = \frac{\tilde{q}}{\tilde{m}} \cdot \frac{\partial_{\tilde{q}} g \cdot \partial_{\tilde{T}_s} f - \partial_{\tilde{q}} f \cdot \partial_{\tilde{T}_s} g}{\partial_{\tilde{T}_s} g \cdot \partial_{\tilde{m}} f - \partial_{\tilde{T}_s} f \cdot \partial_{\tilde{m}} g} \tag{A.10}$$

$$r = \frac{\partial \tilde{T}_s}{\partial \tilde{T}_0} = \frac{\partial_{\tilde{m}} g \cdot \partial_{\tilde{T}_0} f - \partial_{\tilde{m}} f \cdot \partial_{\tilde{T}_0} g}{\partial_{\tilde{T}_s} g \cdot \partial_{\tilde{m}} f - \partial_{\tilde{T}_s} f \cdot \partial_{\tilde{m}} g} \tag{A.11}$$

$$\mu = \frac{1}{\tilde{T}_s - \tilde{T}_0} \frac{\partial \tilde{T}_s}{\partial \ln \tilde{P}} = \frac{\tilde{P}}{\tilde{T}_s - \tilde{T}_0} \cdot \frac{\partial_{\tilde{m}} g \cdot \partial_{\tilde{P}} f - \partial_{\tilde{m}} f \cdot \partial_{\tilde{P}} g}{\partial_{\tilde{T}_s} g \cdot \partial_{\tilde{m}} f - \partial_{\tilde{T}_s} f \cdot \partial_{\tilde{m}} g} \tag{A.12}$$

$$\mu_q = \frac{1}{\tilde{T}_s - \tilde{T}_0} \frac{\partial \tilde{T}_s}{\partial \ln \tilde{q}} = \frac{\tilde{q}}{\tilde{T}_s - \tilde{T}_0} \cdot \frac{\partial_{\tilde{m}} g \cdot \partial_{\tilde{q}} f - \partial_{\tilde{m}} f \cdot \partial_{\tilde{q}} g}{\partial_{\tilde{T}_s} g \cdot \partial_{\tilde{m}} f - \partial_{\tilde{T}_s} f \cdot \partial_{\tilde{m}} g} \tag{A.13}$$

where the notation $\partial_x y$ represents the partial derivatives $\partial y / \partial x$. These partial derivatives are expressed by

$$\partial_{\tilde{T}_0} f = -\frac{\tilde{m}}{C_Q \tilde{Q}_c + \tilde{T}_s - \tilde{T}_0 - f_r J}$$

$$\partial_{\tilde{T}_s} f = \frac{\tilde{m}\tilde{E}_c + f_r J \zeta}{\tilde{E}_c (C_Q \tilde{Q}_c + \tilde{T}_s - \tilde{T}_0 - f_r J)} - \frac{\tilde{m}(2\tilde{T}_s + \tilde{E}_c)}{\tilde{T}_s^2}$$

$$\partial_{\tilde{m}} f = 2\tilde{m} + \frac{f_r J (\tilde{m}\tilde{E}_c - \zeta \tilde{T}_s)}{\tilde{m}\tilde{E}_c (C_Q \tilde{Q}_c + \tilde{T}_s - \tilde{T}_0 - f_r J)} \qquad \partial_{\tilde{P}} f = 0$$

$$\partial_{\tilde{q}} f = \frac{f_r}{C_Q \tilde{Q}_c + \tilde{T}_s - \tilde{T}_0 - f_r J} \tag{A.14}$$

$$\partial_{\tilde{T}_0} g = -1 \qquad \partial_{\tilde{T}_s} g = 1 \qquad \partial_{\tilde{m}} g = \frac{2 x_g \tilde{Q}_g \tilde{m}}{(x_g \tilde{m} + 1)(x_g \tilde{m} + 2)} + \frac{J}{\tilde{m}}$$

$$\partial_{\tilde{P}} g = \frac{-2 x_g \tilde{Q}_g \tilde{m}}{\tilde{P}(x_g \tilde{m} + 1)(x_g \tilde{m} + 2)} \qquad \partial_{\tilde{q}} g = -\frac{1}{\tilde{m}} \tag{A.15}$$

Acknowledgment

This research is supported by the Center for Simulation of Accidental Fires and Explosions (C-SAFE) at the University of Utah, under Lawrence Livermore National Laboratory subcontract B341493.

References

[1] Beckstead, M. W., Davidson, J. E., and Jing, Q., "A Comparison of Solid Monopropellant Combustion and Modeling," *Challenges in Propellants and Combustion: 100 Years after Nobel*, Begell House, New York, 1997, pp. 1116–1132.

[2] Lengelle, G., Duterque, J., and Trubert, J. F., "Physico-chemical Mechanisms of Solid Propellant Combustion," *Solid Propellant Chemistry, Combustion, and Motor Interior Ballistics*, edited by V. Yang, T. B. Brill, and W. Ren, Progress in Astronautics and Aeronautics, AIAA, Reston, VA, 2000, pp. 287–334.

[3] Sell, T., Vyazovkin, S., and Wight, C. A., "Thermal Decomposition Kinetics of PBAN-Binder and Composite Solid Rocket Propellants," *Combustion and Flame*, Vol. 119, Nos. 1–2, 1999, pp. 174–181. doi:10.1016/S0010-2180(99)00036-X

[4] Wang, J., and Wight, C. A., "Thermal Decomposition Kinetics of AP Composite Propellants with HTPB and BAMO-AMMO Binders," *International Journal of Chemical Kinetics* (to be published).

[5] Wang, J., "Investigation of Decomposition Kinetics and Incorporation of Kinetic Models into HMX Combustion Simulation," Ph.D. Dissertation, Chemistry Dept., Univ. of Utah, Salt Lake City, UT, 2005.

[6] Simons, J., "Sponge Model for the Kinetics of Surface Thermal Decomposition of Microcrystalline Solids: Application to HMX," *Journal of Physical Chemistry B*, Vol. 103, No. 41, 1999, pp. 8650–8656. doi:10.1021/jp9842143

[7] Behrens, R., Mack, S., and Wood, J., "Thermal Decomposition Mechanisms of HMX: The Interrelationship of Chemical and Physical Processes," *Proceedings of the 17th JANNAF Propulsion Systems Hazards Subcommittee Meeting*, CPIA681, Vol. 1, JANNAF, 1998, pp. 21–43.

[8] Vyazovkin, S., and Wight, C. A., "Model-Free and Model-Fitting Approaches to Kinetic Analysis of Isothermal and Nonisothermal Data," *Thermochimica Acta*, Vols. 340–341, Dec. 1999, pp. 53–68. doi:10.1016/S0040-6031(99)00253-1

[9] Ward, M. J., Son, S. F., and Brewster, M. Q., "Role of Gas- and Condensed-Phase Kinetics in Burning Rate Control of Energetic Solids," *Combustion Theory and Modelling*, Vol. 2, No. 3, 1998, pp. 293–312. doi:10.1088/1364-7830/2/3/005

[10] Ward, M. J., Son, S. F., and Brewster, M. Q., "Steady Deflagration of HMX with Simple Kinetics: A Gas Phase Chain Reaction Model," *Combustion and Flame*, Vol. 114, Nos. 3–4, 1998, pp. 556–568. doi:10.1016/S0010-2180(97)00332-5

[11] Lengelle, G., "Thermal Degradation Kinetics and Surface Pyrolysis of Vinyl Polymers," *AIAA Journal*, Vol. 8, No. 11, 1970, pp. 1989–1996.

[12] Ibiricu, M. M., and Williams, F. A., "Influence of Externally Applied Thermal Radiation on the Burning Rates of Homogeneous Solid Propellants," *Combustion and Flame*, Vol. 24, No. 2, 1975, pp. 185–198. doi:10.1016/0010-2180(75)90147-9

[13] Brown, M. E., Dollimore, D., and Galwey, A. K., *Reactions in the Solid State. Comprehensive Chemical Kinetics*, Elsevier, Amsterdam, Vol. 22, 1980, Chap. 3, pp. 41–113.

[14] Sestak, J., "Thermophysical Properties of Solids. Their Measurement and Theoretical Thermal Analysis," *Comprehensive Analytical Chemistry*, edited by G. Svehla, Elsevier, Amsterdam, Vol. 12, Pt. D, 1984, Chap. 8.

[15] Opfermann, J., "Kinetic Analysis Using Multivariate Non-Linear Regression, 1: Basic Concepts," *Journal of Thermal Analysis and Calorimetry*, Vol. 60, No. 2, 2000, pp. 641–658. doi:10.1023/A:1010167626551

[16] Son, S. F., and Brewster, M. Q., "Linear Burning Rate Dynamics of Solids Subjected to Pressure or External Radiant Heat Flux Oscillations," *Journal of Propulsion and Power*, Vol. 9, No. 2, 1993, pp. 222–232.

[17] Brewster, M. Q., Ward, M. J., and Son, S. F., "Simplified combustion modeling of double base propellant: gas phase chain reaction vs. thermal decomposition," *Combustion Science and Technology*, Vol. 154, 2000, pp. 1–30.

[18] Zenin, A., "HMX and RDX: Combustion Mechanism and Influence on Modern Double-Base Propellant Combustion," *Journal of Propulsion and Power*, Vol. 11, No. 4, 1995, pp. 752–758.

[19] Tarver, C. M., and Tran, T. D., "Thermal Decomposition Models for HMX-Based Plastic Bonded Explosives," *Combustion and Flame*, Vol. 137, Nos. 1–2, 2004, pp. 50–62. doi:10.1016/j.combustflame.2004.01.002

[20] Brill, T. B., Arisawa, H., Brush, P. J., Gongwer, P. E., and Williams, G. K., "Surface Chemistry of Burning Explosives and Propellants," *Journal of Physical Chemistry*, Vol. 99, No. 5, 1995, pp. 1384–1392. doi:10.1021/j100005a005

[21] Loner, P. S., and Brewster, M. Q., "Oscillatory Laser-Induced Combustion of HMX," *34th JANNAF Combustion Subcommittee Meeting*, CPIA662, Vol. 2, Chemical Propulsion Information Agency, Columbia, MD, 1997, pp. 47–60.

[22] Loner, P. S., and Brewster, M. Q., "On the Oscillatory Laser-Augmented Combustion of HMX," *Proceedings of the 27th Symposium (International) on Combustion*, Vol. 2, The Combustion Inst., Pittsburgh, PA, 1998, pp. 2309–2317.

[23] Kudva, G. N., Lee, Y. J., and Litzinger, T. A., "Study of Pressure and Heat Release Effects on Laser and Pressure-Driven Response Amplitudes for HMX," *37th JANNAF Combustion Subcommittee Meeting*, CPIA701, Vol. 1, Chemical Propulsion Information Agency, Columbia, MD, 2000, pp. 641–652.

[24] Henson, B. F., Smilowitz, L., Asay, B. W., Dickson, P. M., and Howe, P. M., "Evidence for Thermal Equilibrium in the Detonation of HMX," *12th Symposium (International) on Detonation*, Office of Naval Research, Arlington, VA, 2002, pp. 987–995

[25] Atwood, A. I., Boggs, T. L., Curran, P. O., Parr, T. P., Hanson-Parr, D. M., Price, C. F., and Wiknich, J., "Burning Rate of Solid Propellant Ingredients, Part 2: Determination of Burning Rate Temperature Sensitivity," *Journal of Propulsion and Power*, Vol. 15, No. 6, 1999, pp. 748–752.

[26] Atwood, A. I., Boggs, T. L., Curran, P. O., Parr, T. P., Hanson-Parr, D. M., Price, C. F., and Wiknich, J., "Burning Rate of Solid Propellant Ingredients, Part 1: Pressure and Initial Temperature Effects," *Journal of Propulsion and Power*, Vol. 15, No. 6, 1999, pp. 740–747.

[27] Zenin, A. A., and Finjakov, S. V., "Burning-Rate Response Functions of Composite-Modified Double-Base Propellants and HMX," *Solid*

Propellant Chemistry, Combustion, and Motor Interior Ballistics, edited by V. Yang, T. B. Brill, and W. Ren, Progress in Astronautics and Aeronautics, AIAA, Reston, VA, 2000, pp. 639–662.

[28] Novozhilov, B. V., "Theory of Nonsteady Burning and Combustion Stability of Solid Propellants by the Zeldovich-Novozhilov Method," *Nonsteady Burning and Combustion Stability of Solid Propellants*, edited by L. L. Luca, E. W. Price, and M. Summerfield, Progress in Astronautics and Aeronautics, AIAA, Washington, D.C., 1992, pp. 601–641.

[29] Brewster, M. Q., "Solid Propellant Combustion Response: Quasi-Steady (QSHOD) Theory Development and Validation," *Solid Propellant Chemistry, Combustion, and Motor Interior Ballistics*, Progress in Astronautics and Aeronautics, Vol. 185, edited by V. Yang, T. B. Brill, and W. Ren, AIAA, Reston, VA, 2000, Chap 2, pp. 607–637.

[30] DeLuca, L., "Theory of Nonsteady Burning and Combustion Stability of Solid Propellants by Flame Models," *Nonsteady Burning and Combustion Stability of Solid Propellants*, edited by L. L. Luca, E. W. Price, and M. Summerfield, Progress in Astronautics and Aeronautics, AIAA, Washington, D.C., 1992, pp. 519–600.

[31] DeLuca, L., Silvestro, R. D., and Cozzi, F., "Intrinsic Combustion Instability of Solid Energetic Materials," *Journal of Propulsion and Power*, Vol. 11, No. 4, 1995, pp. 804–815.

[32] Finlinson, J. C., Stalnaker, R. A., and Blomshield, F. S., "HMX and RDX T-Burner Pressure Coupled Response from 200 to 1000 PSI," *36th Aerospace Sciences Meeting and Exhibit*, AIAA Paper No. 98-0556, 1998.

[33] Erikson, W. W., and Beckstead, M. W., "Modeling Pressure and Heat Flux Responses of Nitramine Monopropellants with Detailed Kinetics," *35th JANNAF Combustion Subcommittee Meeting*, Chemical Propulsion Information Agency, Columbia, MD, 1998, pp. 415–434.

[34] Cozzi, F., DeLuca, L. T., and Novozhilov, B. V., "Linear Stability and Pressure-Driven Response Function of Solid Propellants with Phase Transition," *Journal of Propulsion and Power*, Vol. 15, No. 6, 1999, pp. 806–815.

[35] Liau, Y. C., Kim, E. S., and Yang, V., "A Comprehensive Analysis of Laser-Induced Ignition of RDX Monopropellant," *Combustion and Flame*, Vol. 126, No. 3, 2001, pp. 1680–1698. doi:10.1016/S0010-2180(01)00281-4

[36] Kim, E. S., Yang, R., and Yang, V., "Modeling of Nitramine Propellant Combustion and Ignition," *Energetic Materials: Initiation, Decomposition and Combustion*, edited by P. Politzer, Theoretical and Computational Chemistry Series, Academic Press/Elsevier Science, New York, 2003, pp. 295–350.

[37] Gusachenko, L. K., Zarko, V. E., and Rychkov, A. D., "Effect of Melting on Dynamic Combustion Behavior of Energetic Materials," *Journal of Propulsion and Power*, Vol. 15, No. 6, 1999, pp. 816–822.

[38] Washburn, E. B., Beckstead, M. W., and Gross, M. L., "Condensed-Phase Model for HMX Decomposition," *38th JANNAF Combustion Subcommittee Meeting*, Chemical Propulsion Information Agency, Columbia, MD, 2002, pp. 33–42.

[39] Margolis, S. B., and Williams, F. A., "Diffusional/Thermal Coupling and Intrinsic Instability of Solid Propellant Combustion," *Combustion Science and Technology*, Vol. 59, Nos. 1–3, 1988, pp. 27–84. doi:10.1080/00102208808947089

[40] Margolis, S. B., and Williams, F. A., "Influence of Porosity and Two-Phase Flow on Diffusional/Thermal Instability of a Deflagrating Energetic Material," *Combustion Science and Technology*, Vol. 106, Nos. 1–3, 1995, pp. 41–68. doi:10.1080/00102209508907766

[41] Murphy, J. J., "Modeling of the Linear Burning Rate Response of Solid Propellants to Pressure Oscillations," M.S. Dissertation, Dept. of Mechanical and Industrial Engineering, Univ. of Illinois, Urbana-Champaign, IL, 1998.

S. Son
Associate Editor